IEEE Access
Multidisciplinary ⋮ Rapid Review ⋮ Open Access Journal

Received 28 March 2024, accepted 3 May 2024, date of publication 13 May 2024, date of current version 20 May 2024.

Digital Object Identifier 10.1109/ACCESS.2024.3400684

RESEARCH ARTICLE

A Novel Sliding Hysteresis Band Based Direct Torque Control Scheme for PMSM Motors to Achieve Improved Current THD With Reduction in Torque and Flux Ripples Eliminating the Low-Speed Problems

ANJALY MOHAN[1], (Student Member, IEEE), MEERA KHALID[1], AND A. C. BINOJKUMAR[2], (Senior Member, IEEE)
[1]Rajiv Gandhi Institute of Technology, APJ Abdul Kalam Technological University, Thiruvananthapuram, Kerala 695016, India
[2]Government Engineering College Idukki, APJ Abdul Kalam Technological University, Thiruvananthapuram, Kerala 695016, India

Corresponding author: Anjaly Mohan (anjalymohan90@gmail.com)

ABSTRACT The performance of Direct Torque Controlled (DTC) Permanent Magnet Synchronous Motor (PMSM) is severely hampered by high Total Harmonic Distortion (THD) in motor current, especially under low-speed operations. Current THD problems show up as torque ripple, elevated losses, temperature rise, low power factor, and shorter motor lifetime. In DTC, the effects of high THD are magnified, necessitating an in-depth study of the challenges and its mitigating techniques. In this paper, novel sliding bands are proposed for torque and flux hysteresis controllers to improve the current THD with a special focus on low-speed regions. The proposed DTC schemes offer smooth low-speed operation with only a marginal increase in switching frequency. Even though the low-speed region is the targeted operating region, a significant THD reduction is seen over the whole operating region, with the added benefit of torque ripple and flux ripple reduction. The effectiveness of the proposed scheme is analytically and experimentally verified on a 1.07 kW PMSM drive. The proposed schemes exhibit better performance in comparison with the conventional methods, especially under low-speed regions, and significantly improve the low-speed performance.

INDEX TERMS Current THD, DTC, flux ripple, low-speed problem, PMSM, sliding band, SVPWM, torque ripple.

I. INTRODUCTION

Permanent Magnet Synchronous Motors (PMSMs) have grown to be a key component of electric propulsion and industrial automation, potentially redefining efficiency and accuracy in motion control. Space Vector Modulated Field Oriented Control (SVM FOC) is a commonly adopted control strategy in PMSM drives. Takahashi [1] introduced Direct Torque Control (DTC) for high-performance electric drives which gained much attention due to the simple implementation and quick dynamic response. Despite having many advantages for the SVM FOC scheme, the conventional DTC scheme is preferred due to the noted advantages like the absence of coordinate transformations, use of a single PI controller and resulting faster response, direct control over torque and flux ripples, improved dynamic performance, and decreased susceptibility to changes in parameters and uncertainties in the system. This real-time control provides direct and accurate control over torque and flux without the need for complex control algorithms, enabling PMSMs to respond quickly to dynamic variations in load and speed.

Even though conventional DTC is simple to implement, it shows high current THD under low-speed operating conditions. Current THD reflects the distortion, which is

The associate editor coordinating the review of this manuscript and approving it for publication was Feifei Bu.

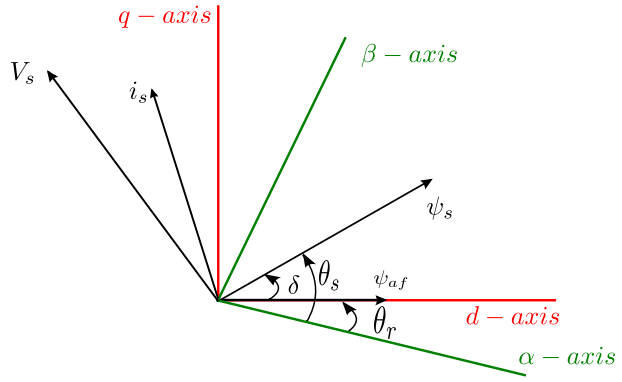

FIGURE 1. Alignment of different vectors used in d-q and $\alpha-\beta$ frames.

represented by the amount of undesirable harmonics that depart from the fundamental frequency, in the current waveform applied to the PMSM. To reduce THD and improve motor performance, several techniques, including modulation methods, filter designs, and optimization algorithms have been reported.

The ability of the Space Vector Modulation (SVM) scheme to produce almost sinusoidal current waveforms and its intrinsic capability to lower THD make it particularly well-liked. Lascu et al. [2] suggested combining the DTC scheme with the Space vector PWM technology, also referred to as the SVM-based DTC scheme to maintain constant switching frequency. This technique replaces the torque hysteresis controller in the inner loop with a torque PI controller. The lookup table and flux hysteresis controller are eliminated, and the reference voltage vector is generated using the Space Vector modulation technique. During steady-state operation, it can reduce ripples in torque, flux, current, and speed pulsations along with acoustic noise suppression. With this method, the switching frequency is kept constant; however, the flexibility to manage the torque ripple and flux ripple is lost and the number of PI controllers is increased to three. A similar implementation is proposed by Lai et al. in [3].

Many modifications to the conventional SVM-based DTC method are reported in the literature. Using a reference flux vector calculator, the reference stator flux linkage vector is determined in [4]. This work focuses on the flux-weakening zone of operation, where ripples in torque and flux are significantly decreased. In addition to rotational coordinate transformation, the SVM-based DTC systems thus developed require three PI controllers. Since PI controller tuning is an extremely challenging task, the drive system becomes more complex to design. The system's transient performance is also impacted by the addition of more PI controllers. In reference [5], a novel approach utilizing a single PI controller is proposed, hence eliminating the complexity of three PI controllers. However, flux updating is inaccurate owing to the assumptions in [5]. Moreover, this approach is parameter-dependent and does not account for loss reduction.

To reduce current THD, SVM-based DTC with several PWM techniques such as Hysteresis-Based PWM and Space Vector Modulation (SVM) have been reported in the literature. SVM optimizes its voltage vectors to reduce the error between the flux /torque and its corresponding references. As a result, the harmonic content of the motor phase currents is reduced [6]. Hybrid modulation approaches, such as Carrier-Based PWM with Phase-Shifted Disposition (CB-PSPWM), which combines Carrier-Based PWM with phase-shifting, are presented in [7] to further improve THD reduction. In these methods, the ease of the DTC scheme is lost along with the freedom of adjusting the torque and flux ripples. Further, these methods require extra PI controllers, making the system harder to build.

Furthermore, it is discovered that adding a multilevel inverter to a DTC-based control system lowers distortion in current [8], [9], [10]. Researchers have looked into several multilevel inverter topologies, including Neutral-Point Clamped (NPC) and Cascaded H-Bridge inverters. Although multilevel inverters are more often used in PMSM-DTC systems; they can be expensive and the control is complex.

Adding more levels to the torque hysteresis controller has been the subject of numerous works of literature [11]. Also, there is a requirement for more voltage vectors with the increment of levels in the hysteresis comparator, which cannot be provided by the conventional two-level inverter, and hence its application is constrained. The conventional DTC has a legitimate dynamic response but is ineffective at low speeds. To solve this problem, Zahraoui et al. [12] proposed a zone-shifting approach that modifies the switching table and sectors in the conventional DTC, raising the fundamental value of inverter output voltage and enhancing the dynamic performance with a reduction in torque pulsation, flux distortion, and total harmonic distortion. Although the phase current THD is decreased, the THD is still at a higher value. By combining matrix converter and DTC without adding new levels to hysteresis comparators, Cassedi et al. [13] achieved a reduction of current THD. The potential for using matrix converters to make use of multilevel hysteresis comparators' advantage is addressed in [14] and [15]. Nordan et al. suggested a 5-level cascaded H-bridge multilevel inverter topology in [16], where multilevel hysteresis comparators are fitted to the torque hysteresis comparator to lower the stator current THD as well as torque and flux ripples. With two new look-up tables in [17], a model predictive control for matrix converter results in less torque ripple and consequently less current THD. All of the aforementioned methods lose the simplicity of the DTC approach because these require matrix converters, and hence become complex. Further, the use of more number of switches increases switching loss and complicates the control. The lack of voltage vectors has also hindered research into multilevel hysteresis comparators with conventional 2-level inverters.

The DTC-based PMSM motors are used in multiple fields for accurate control [18] under no-load conditions, including automated guided vehicles, solar tracking systems, antenna positioning in satellite communication, laboratory and research equipment, and semiconductor manufacturing

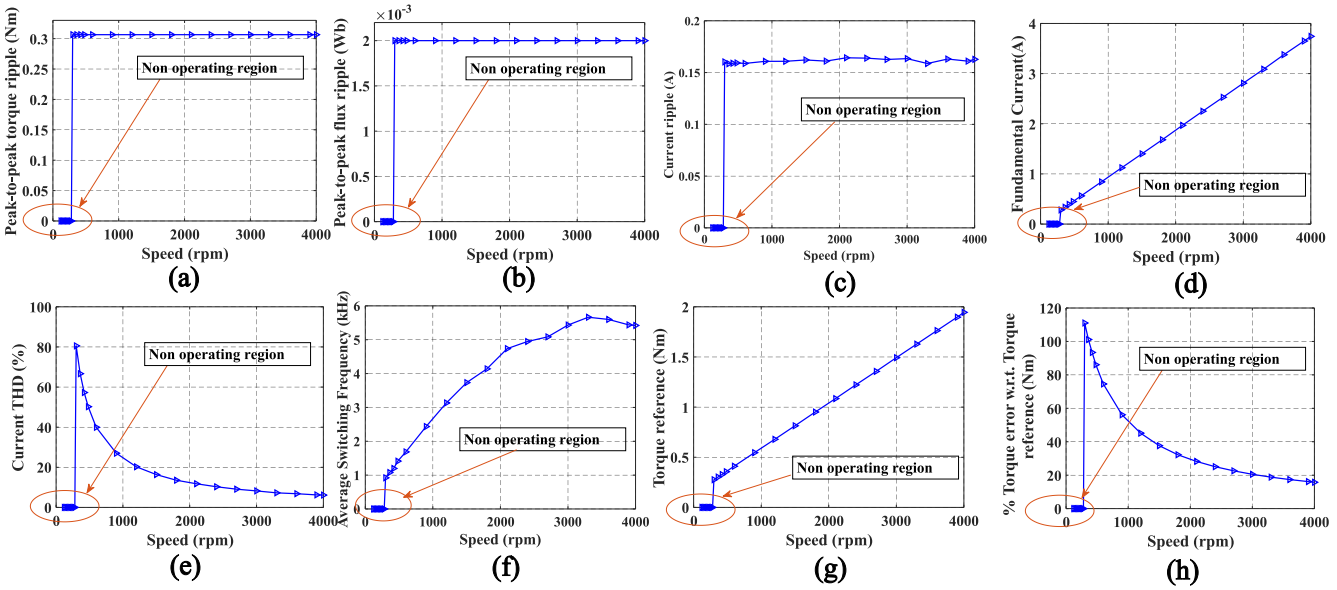

FIGURE 2. Performance parameters of conventional DTC scheme under no-load condition with the torque band= 12% of rated torque and flux band = 0.001 Wb (a) Peak-to-peak torque ripple (b) Peak-to-peak flux ripple (c) Peak-to-peak current ripple (d) Fundamental current (e) Average switching frequency (f) % Current THD (g) Torque reference (h) % Torque error w.r.t. Torque reference.

equipment. So, this paper addresses the high current THD problem of DTC-based PMSM motors operated under no load.

The major highlights of the work are:

- Small-signal model of PMSM is derived in terms of torque ripple, flux ripple, voltage ripple, and current ripple.
- The low-speed running problem associated with the conventional DTC scheme is addressed through the sliding of torque and flux hysteresis bands.
- A computationally simple equation for systematically sliding the bands of torque and flux hysteresis comparator pertaining to DTC is proposed, to achieve the lowest feasible current THD without significantly increasing the switching frequency.
- The proposed methods are experimentally validated on a 1.07 kW PMSM motor drive with WAVECT- FPGA controller.

II. COMPREHENSIVE INSIGHT INTO THE CONVENTIONAL DIRECT TORQUE CONTROL OF PMSM

In this paper, a surface-mounted PMSM (SPMSM) is considered, and the corresponding torque equation given by [19],

$$T_e = \frac{3}{2}\frac{P}{2L_s}\psi_{af}|\psi_s|sin\delta \tag{1}$$

where ψ_s is the stator flux linkage, P is the number of poles, ψ_{af} is the rotor flux linkage, δ is the torque angle, and L_s is the stator inductance respectively. The alignment of different vectors used with PMSM in d-q and $\alpha-\beta$ frames is exhibited in Fig.1. In conventional DTC, the required electromagnetic

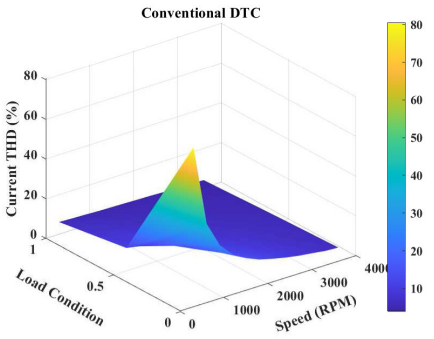

FIGURE 3. Comparison of current THD in stator current for different load conditions for Conventional DTC scheme.

torque is obtained by controlling the magnitude of stator flux and torque angle δ given in (1). The torque and flux hysteresis comparators in DTC limit the respective errors within the specified band.

Despite being exceptionally simple, the conventional DTC scheme nevertheless encounters several shortcomings including significant torque ripple and high current THD under low speed.

In Fig.2, a comparison of the different performance parameters of conventional DTC, with a torque band of 12% rated torque and 0.001 Wb flux band (0.6% of rated flux) for different speeds under no-load conditions is depicted. Since the bands are fixed for the entire operating region, the peak-to-peak torque ripple and peak-to-peak flux ripple are seen as constant as given in Fig.2a and Fig.2b respectively. The current ripple is found to be constant as shown in Fig.2c, and its relation with torque ripple and flux ripple is investigated in the coming section.

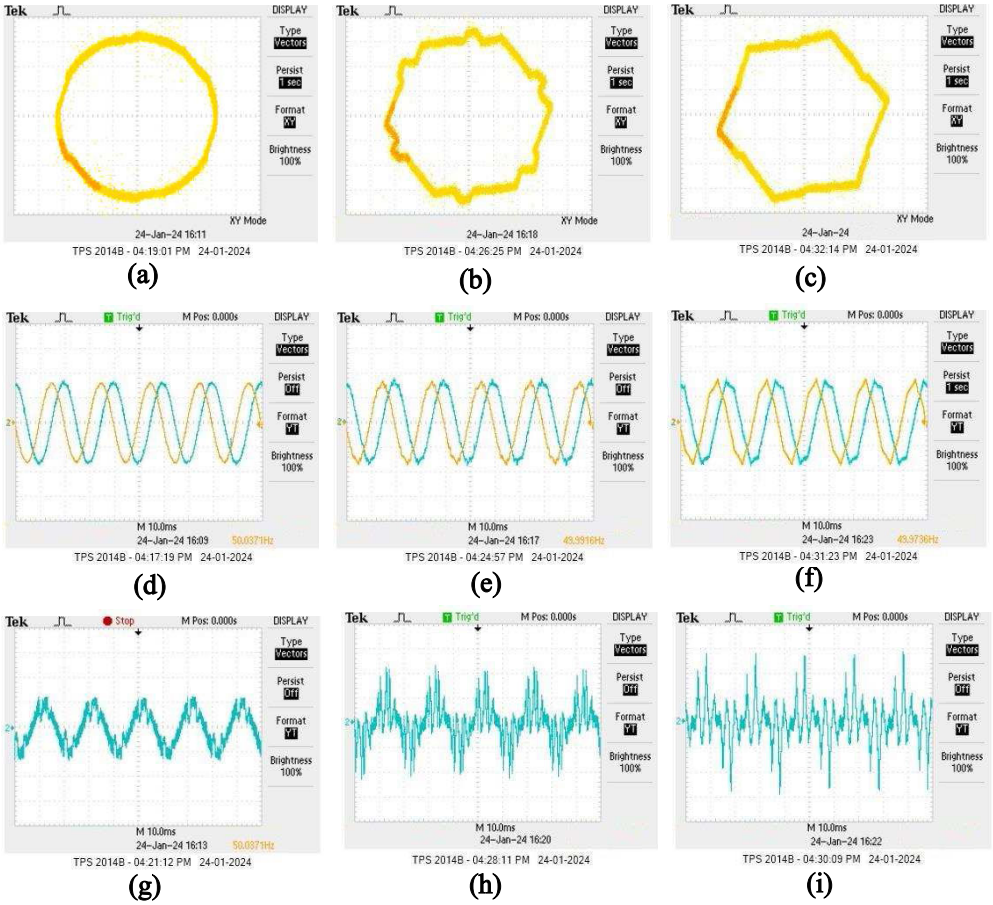

FIGURE 4. Experimentally obtained stator flux trajectory, stator flux in $\alpha - \beta$ frame and the corresponding current waveform for conventional DTC at 1500 rpm (a),(d) and (g) flux band = 0.6% of rated flux (b), (e) and (h) flux band = 6% of rated flux(c), (f) and (i) flux band = 9% of rated flux.

The current THD is affected by current ripple and fundamental current as given in (2)

$$i_{THD} = \frac{1}{i_{s1}} \sqrt{\sum_{n=2}^{\infty} (i_n)^2} = \frac{\widetilde{i_s}}{i_{s1}}. \tag{2}$$

where i_{s1} is the fundamental stator current and $\widetilde{i_s}$ is the current ripple. For a constant value of current ripple ($\widetilde{i_s}$), current THD depends on the magnitude of fundamental current (i_{s1}). i_{s1} is affected by various operating conditions and is detailed below:

The fundamental torque expression is given by,

$$T_e = J\frac{d\omega_m}{dt} + B\omega_m + T_l \tag{3}$$

where T_e is the developed torque, J is the moment of inertia, ω_m is the speed in mechanical rad/sec, B is the viscous friction coefficient and T_l is the load torque. Under steady-state conditions,

$$T_e = B\omega_m + T_l. \tag{4}$$

That is, any increase in speed under the same load conditions requires an increament in T_e. Similarly, the application of load T_l on the motor, under the same speed conditions needs corresponding changes in T_e. So, changes in T_e are reflected in the fundamental current (i_{s1}) and current THD. Therefore, as the speed advances, the motor draws more current, and hence the fundamental current increases as seen in Fig.2d. Compared to the fundamental current, the current ripple is high as far as the low-speed region is concerned which leads to a high current THD at the low-speed region as seen in Fig.2e. Due to this, the motor is unable to run at the low-speed region up to 300 rpm. The torque reference for different speed conditions is given in Fig.2g and is found to be increasing linearly as the speed increases. Fig.2h depicts the % torque error w.r.t. the reference torque for different speed conditions. Since the peak-to-peak torque ripple is constant throughout the entire speed range, the % torque error is very high in the low-speed region. Upon verification, it is seen that the torque error is reflected in the ripple component of the stator current. So, the rms harmonic/ripple in the stator current has to be reduced to decrease the stator current THD. The current THD for the entire operating region with no-load, half load and full load condition is given in Fig.3. It is seen that the current THD decreases with increasing speed and also decreases when the motor is loaded. So, the problem of high

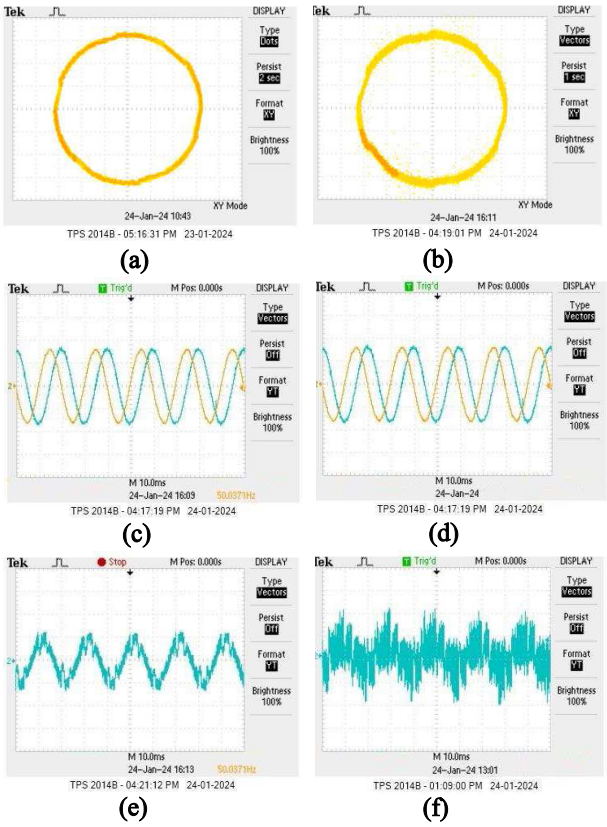

FIGURE 5. Experimentally obtained stator flux trajectory, stator flux in $\alpha - \beta$ frame and the corresponding current waveform for flux band = 0.6% for conventional DTC at (a),(c) and (e) 1500 rpm (b), (d) and (f) 300 rpm.

THD is predominant in the low speed region under light load conditions.

It is known that the torque hysteresis band contributes significantly to the switching frequency, whereas the flux hysteresis band mainly affects the current THD [20]. The second part of the above statement is experimentally verified and presented in Fig.4. The stator flux band has a significant effect on the shape of the current waveform, and a sinusoidal current waveform with low harmonic content demands a circular flux trajectory. Fig.4a-c shows the stator flux trajectory for the conventional DTC scheme with flux bands of 0.6%, 6%, and 9% of the rated stator flux. Fig.4d-f shows the corresponding flux in $\alpha - \beta$ axis and Fig. 5g-i shows its current waveform. It is seen that as the flux band narrows, the flux trajectory is observed to become more circular, and hence the current waveform resembles a near-sine wave. Further, it is found that the speed of operation affects the current waveform with the same flux band. Experimentally obtained stator flux trajectory, stator flux in $\alpha - \beta$ frame, and the corresponding current waveform for conventional DTC at 1500 rpm and 300 rpm are presented in Fig. 5 for a flux band of 0.6% of rated flux. The current waveform becomes more and more distorted as the speed reduces and the THD is measured as 16.37% at 1500 rpm whereas it is increased to 80.54% for 300 rpm.

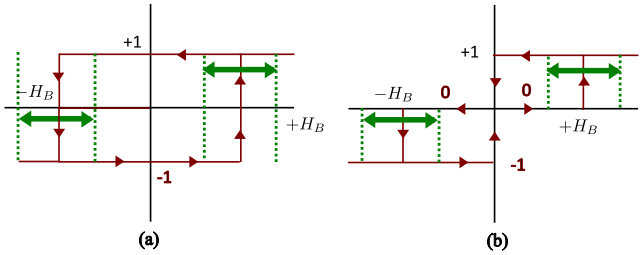

FIGURE 6. Concept of the modification in the hysteresis band (a) flux hysteresis controller (b) Torque hysteresis controller.

From the detailed analysis of the conventional DTC scheme presented in this section, the following conclusions are drawn:

- Compared to high-speed zones, the current THD is extremely high during the low-speed regions. The existence of a constant rms current ripple and a reduced fundamental component of current during low-speed operation results in an upsurge in THD.
- Due to the presence of high current THD and high percentage torque error, the motor is unable to run in very low-speed ranges.

The high current THD problem and subsequent low-speed running problems are addressed in this paper by logically sliding the bands of both the torque and flux hysteresis controllers.

III. PROPOSED METHODOLOGY

In conventional DTC scheme, the flux error and torque error are maintained within stipulated bands and are kept constant throughout the range of operation. Due to this, flux ripple ($\tilde{\psi}_s$) and torque ripple ($\tilde{T}_e$) are constant. In this paper, the flux and torque hysteresis bands are made sliding to lower the current THD, as illustrated in Fig.6. Determination of the sliding pattern for both flux and torque bands under different operating conditions is a challenging task. To choose the hysteresis bands of the DTC for the PMSM, Mathapati et al. provided an analytical and offline method [21], but it is computationally complex, and the base time required for the calculation relies on various aspects, such as speed, and is not taken into account. Additionally, all feasible flux and torque controller band combinations for the required state are determined, and the combination matching the desired condition is chosen. However, these are motor-specific and cannot be generalized. It is a time-consuming strategy, as the author mentioned in his paper. Therefore, a simple and effective way of band variation is proposed and investigated thoroughly in the coming sections.

A. SMALL SIGNAL MODELLING OF CURRENT RIPPLE IN PMSM

To effectively address the problem of high current THD, an in-depth theoretical investigation of the variables influencing the current THD is necessary. This can be deduced from the fundamental model of the PMSM in the d-q rotor

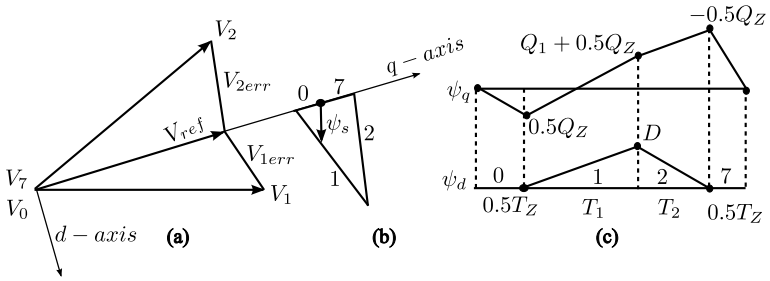

FIGURE 7. (a) Instantaneous voltage error vectors corresponding to conventional SVPWM switching sequence 0-1-2-7 in sector 1 (b) Trajectory of flux ripple (c) Flux ripple along d and q axi.

reference frame described by,

$$V_d = R_s i_d + \frac{d\psi_d}{dt} - \omega_s \psi_q \tag{5}$$

$$V_q = R_s i_q + \frac{d\psi_q}{dt} + \omega_s \psi_d \tag{6}$$

where V_d and V_q, i_d and i_q, ψ_d and ψ_q are the stator voltage, stator current, and flux in the d-q axes respectively. R_s is the stator resistance and ω_s is the motor speed. Under steady-state conditions, (5) and (6) are rearranged as follows:

$$V_d = R_s i_d - \omega_s \psi_q \tag{7}$$

$$V_q = R_s i_q + \omega_s \psi_d. \tag{8}$$

The magnitude of the stator voltage is given by,

$$V_s{}^2 = V_d^2 + V_q^2 \tag{9}$$

where V_s is the magnitude of the stator voltage vector, V_s. substituting (7) and (8) in (9) gives,

$$V_s{}^2 = R_s^2 \left[i_d^2 + i_q^2\right] + \omega_s^2 \left[\psi_d^2 + \psi_q^2\right] + 2\omega_s R_s \left[\psi_d i_q - \psi_q i_d\right] \tag{10}$$

$$V_s{}^2 = R_s^2 i_s^2 + \omega_s^2 \psi_s^2 + 2\omega_s R_s \frac{4T_e}{3P} \tag{11}$$

where i_s and ψ_s are the magnitudes of stator current vector i_s and stator flux vectors $\boldsymbol{\psi_s}$. Applying a small perturbation in (11),

$$(V_s+\tilde{V_s})^2 = R_s^2(i_s+\tilde{i_s})^2 + \omega_s^2(\psi_s+\tilde{\psi_s})^2 + 2\omega_s R_s \frac{4(T_e+\tilde{T_e})}{3P}. \tag{12}$$

Subtracting (12) from (11) and neglecting the square terms of ripple,

$$V_s\tilde{V_s} = R_s^2 i_s \tilde{i_s} + \omega_s^2 \psi_s \tilde{\psi_s} + \omega_s R_s \frac{4\tilde{T_e}}{3P}. \tag{13}$$

Equation (13) provides a crucial relation and shows that $\tilde{\psi_s}$ and $\tilde{T_e}$ contribute to stator voltage ripple ($\tilde{V_s}$) and hence result in stator current ripple ($\tilde{i_s}$). These factors, along with the speed information, are used in this paper to reduce the current THD given by (2). Further, stator flux ψ_s is given by,

$$\boldsymbol{\psi_s} = L_s \boldsymbol{i_s} + \psi_{af} \tag{14}$$

Applying a small perturbation in (14) results in,

$$\tilde{\psi_s} = L_s \tilde{i_s}. \tag{15}$$

Also, the developed torque of SPMSM is given by,

$$T_e = \frac{3}{2}\frac{P}{2}\psi_{af} i_q. \tag{16}$$

Applying small perturbations to the (16) gives,

$$T_e + \tilde{T_e} = \frac{3}{2}\frac{P}{2}\psi_{af}(i_q + \tilde{i_q}). \tag{17}$$

The difference between (16) and (17) gives the torque ripple and is given as,

$$\tilde{T_e} = \frac{3}{2}\frac{P}{2}\psi_{af}\tilde{i_q}. \tag{18}$$

From (13), (15), and (18), it is noted that the stator current ripple ($\tilde{i_s}$), flux ripple ($\tilde{\psi_s}$), torque ripple ($\tilde{T_e}$), and voltage ripple ($\tilde{V_s}$) are interrelated and different possibilities are analyzed in Table 1. Only one possibility is detailed and the same analysis can be extended to other cases. Out of 4 possible combinations of $\tilde{T_e}$ and $\tilde{\psi_s}$, increment in $\tilde{T_e}$ with constant $\tilde{\psi_s}$, for instance, is referred to as the first condition. Under such circumstances, $\tilde{V_s}$ remains constant if and only if $\tilde{i_s}$ is reduced by the same amount as given by (13). This is because both $\tilde{T_e}$ and $\tilde{i_s}$ fall on the right-hand side of (13). In the second row, a constant $\tilde{i_s}$ is obtained if $\tilde{V_s}$ increases suitably (refer (13)). However, it is inferred from (15) and (18) that both $\tilde{\psi_s}$ and $\tilde{T_e}$ are directly related to $\tilde{i_s}$. i.e, an increase in $\tilde{\psi_s}$ or $\tilde{T_e}$ or both leads to an increment in $\tilde{i_s}$. Therefore, the above two conditions are rejected. The third row shows an increase in both $\tilde{V_s}$ and $\tilde{i_s}$ for the same input conditions and can be accepted. In Table.1, all the possibilities are shown, and accepted cases are shaded. It is inferred that an increase in $\tilde{T_e}$ or $\tilde{\psi_s}$, or both may be a contributing factor to the rise of $\tilde{V_s}$ and $\tilde{i_s}$. In effect, a significant reduction in $\tilde{i_s}$ is achieved by decreasing $\tilde{T_e}$ or $\tilde{\psi_s}$ by narrowing the torque band/flux band. In this paper, both the torque band and flux band are reduced simultaneously to improve the current THD, especially under low motor speed.

Other topologies employ intricate calculations and new candidate voltage vectors to address the high current THD problem in a convoluted manner. This difficulty is resolved

TABLE 1. Effect of flux ripple ($\tilde{\psi}_s$) and torque ripple ($\tilde{T}_e$) on voltage ripple ($\tilde{V}_s$) and current ripple ($\tilde{i}_s$).

$\tilde{T}_e$	$\tilde{\psi}_s$	$\tilde{V}_s$	$\tilde{i}_s$	Remarks
	–	–	↓	Rejected
↑	–	↑	–	Rejected
	–	↑	↑	Accepted
	–	–	↑	Rejected
↓	–	↓	–	Rejected
	–	↓	↓	Accepted
–		–	↓	Rejected
–	↑	↑	–	Rejected
–		↑	↑	Accepted
–		–	↑	Rejected
–	↓	↓	–	Rejected
–		↓	↓	Accepted

↑ Increment
↓ Decrement
– No change

in this paper without sacrificing the simplicity of the conventional DTC scheme, and no additional computing effort is imposed.

B. ANALYTICAL EVALUATION OF STATOR FLUX BAND VARIATION PROPOSED

The sliding of the torque band and flux band adopted in this paper is based on the conventional space vector PWM (SVPWM)-based FOC (Field oriented control) technique, as FOC performs better than conventional DTC under low-speed motor operation [22]. The use of voltage vectors by the inverter to realize a specific reference voltage ($\mathbf{V_{ref}}$) in SVPWM causes instantaneous voltage error, and this results in ripples in the stator flux. This can be seen in the current THD and is indicative of the current ripple. Fig.7 illustrates the voltage error vectors and consequent stator flux ripple vector along the d and q axes, which correspond to the conventional SVPWM switching sequence 0-1-2-7 in sector 1.

The error voltage vectors V_{1err}, V_{2err}, and V_{zerr} resulting from the application of the voltage vectors, V_1 and V_2, and V_z are given by [22], [23], and [24]

$$\mathbf{V_{1err}} = \mathbf{V_1} - \mathbf{V_{ref}} \tag{19}$$

$$\mathbf{V_{1err}} = sin(\alpha) + j[cos(\alpha) - V_{ref}] \tag{20}$$

$$\mathbf{V_{2err}} = \mathbf{V_2} - \mathbf{V_{ref}} \tag{21}$$

$$\mathbf{V_{2err}} = -sin(60^\circ - \alpha) + jcos[(60^\circ - \alpha) - V_{ref}] \tag{22}$$

$$\mathbf{V_{zerr}} = -\mathbf{V_{ref}} = -jV_{ref} \tag{23}$$

Angle made by $\mathbf{V_{ref}}$ with the beginning of the sector 1 is denoted by α. The stator flux ripple ($\tilde{\psi}_s$) throughout a sub-cycle is calculated by taking the error volt-second balance by multiplying (20) to (23) by the appropriate dwell periods T_1, T_2, T_z, and taking the sum of these. Equations (24) and (25), as shown at the bottom of the next page, provide the q-axis flux ripple ($\tilde{\psi}_q$) and d-axis flux ripple ($\tilde{\psi}_d$) respectively for the switching sequence 0-1-2-7. Over a sub-cycle, the mean square flux ripple in q- axis and d-axis ($\tilde{\psi}_q{}^2$) and ($\tilde{\psi}_d{}^2$) is given by,

$$\begin{aligned}\tilde{\psi}_q{}^2 = {} & \frac{1}{3}(0.5Q_Z)^2\frac{T_Z}{2T_s} + \frac{1}{3}[(0.5Q_Z)^2 \\ & + 0.5Q_Z(0.5Q_Z + Q_1) + (0.5Q_Z + Q_1)^2]\frac{T_1}{T_s} \\ & + \frac{1}{3}[(0.5Q_Z + Q_1)^2 - (0.5Q_Z + Q_1)0.5Q_Z \\ & + (-0.5Q_Z)^2]\frac{T_2}{T_s} + \frac{1}{3}(-0.5Q_Z)^2\frac{T_Z}{2T_s}\end{aligned} \tag{26}$$

$$\tilde{\psi}_d{}^2 = \frac{1}{3}D^2\frac{[T_1 + T_2]}{T_s} \tag{27}$$

where,

$$t_a = t - 0.5\,T_z,\ t_b = t - 0.5\,T_z - T_1$$

and $t_c = t - 0.5\,T_z - T_1 - T_2$

$$T_1 = V_{ref} * T_s\frac{sin(60^\circ - \alpha)}{sin60^\circ} \tag{28}$$

$$T_2 = V_{ref} * T_s\frac{sin(\alpha)}{sin60^\circ} \tag{29}$$

$$T_z = T_s - T_1 - T_2 \tag{30}$$

$$\begin{aligned}C_1 = {} & \frac{2}{3\sqrt{(3)}}cos(30 - \alpha)[-\frac{1}{2} + \frac{1}{3}sin^2(30 - \alpha) \\ & - \frac{4}{3}sin^4(30 - \alpha) + \frac{4}{3}sin^2(60 - \alpha)sin^2\alpha]\end{aligned} \tag{31}$$

$$\begin{aligned}C_2 = {} & \frac{1}{3}[\frac{1}{3} + \frac{2}{3}sin^2(30 - \alpha) \\ & - \frac{4}{3}sin^2(30 - \alpha)cos^2(30 - \alpha)]\end{aligned} \tag{32}$$

$$Q_1 = (cos\alpha - V_{ref})T_1, \quad Q_2 = [cos(60 - \alpha) - V_{ref}]T_2 \tag{33}$$

$$Q_Z = -V_{ref}T_Z \quad \text{and} \quad D = sin(\alpha)T_1 \tag{34}$$

The stator flux ripple is given by,

$$\tilde{\psi}_s = \sqrt{\frac{1}{12}T_s^2V_{ref}^2 + C_1T_s^2V_{ref}^3 + C_2T_s^2V_{ref}^4}. \tag{35}$$

It is seen from (35) that, the stator flux ripple is a function of V_{ref} expressed in per unit and T_s, where, V_{ref} and ω_s are closely related as shown below:
The modulation index is given by,

$$m_a = \frac{\widehat{V}_{mod}}{\widehat{V}_{car}} \tag{36}$$

where $\widehat{V}_{mod}$ and $\widehat{V}_{car}$ are the peak amplitude of the modulating signal and the carrier signal respectively. Also,

$$\widehat{V}_{mod} \propto \omega_s \tag{37}$$

$$\widehat{V}_{mod} \propto V_{ref} \propto \omega_s. \tag{38}$$

Hence, it can be seen that V_{ref} is controlling the motor speed. Fig.8 demonstrates the variation of rms flux ripple ($\tilde{\psi}_s$), rms d-axis flux ripple ($\tilde{\psi}_d$), and rms q-axis flux ripple ($\tilde{\psi}_q$) ripple within a sector for two different V_{ref}. Fig.8a is plotted for $V_{ref} = 0.866$ pu (4000 rpm) corresponding to the rated condition and Fig.8b pertaining to $V_{ref} = 0.065$ pu

corresponding to low-speed (300 rpm). It can be inferred from the two plots that the d-axis flux ripple ($\tilde{\psi}_d$) is the dominating component in the high-speed region whereas, the q-axis flux ripple ($\tilde{\psi}_q$) is dominating in the low-speed region. Another important observation from the same figure is that, $\tilde{\psi}_s$, $\tilde{\psi}_d$, and $\tilde{\psi}_q$ are very much affected by the variation in V_{ref}, and also the value varies with the angle α. The maximum rms flux ripple under different speeds can be analytically calculated as,

$$\frac{d\tilde{\psi}_s}{dV_{ref}} = 0 \tag{39}$$

i.e,

$$4C_2V_{ref}^2 + 3C_1V_{ref} + \frac{1}{6} = 0 \tag{40}$$

This is a second-order equation in V_{ref} and the solution is complex with transcendental terms and hence increases the computational burden. So, in this paper, a simple method is adopted to obtain the flux band for every operating condition. Fig.8c gives the variation of $\tilde{\psi}_s$ over a sector for different V_{ref} and upon analyzing the pattern, it is clear that the maximum value of stator flux occurs exactly at an angle of 30°. The flux pattern for FOC shows the exact pattern as predicted by the analytical equation and is given in Fig.8d along with its sector information in Fig.8e. So, by simply equating $\alpha = 30°$ in C_1 and C_2 given in (31) and (32) gives,

$$C_1 = -\frac{5}{18\sqrt{3}} = -0.16039 \quad , \quad C_2 = \frac{1}{9} = 0.111. \tag{41}$$

Substituting this value in (35) gives the simple expression for $\tilde{\psi}_s$ which depends only on V_{ref} and T_s and is given by,

$$\tilde{\psi}_s = \sqrt{\frac{1}{12}T_s^2V_{ref}^2 - \frac{5}{18\sqrt{3}}T_s^2V_{ref}^3 + \frac{1}{9}T_s^2V_{ref}^4} \tag{42}$$

where T_s is always constant corresponding to a switching frequency of 6 kHz as used in FOC. Since V_{ref} is the only variable parameter in (42) and is expressed in per unit quantity, this generalized equation can be used for any type of motor with any capacity. The analytically calculated maximum value of $\tilde{\psi}_s$ for different speed conditions are plotted in Fig.8f and is used as the pattern of flux band variations in the proposed method.

C. ANALYTICAL EVALUATION OF TORQUE BAND VARIATION PROPOSED

From (18), it is seen that the torque ripple is reflected in $\tilde{i_q}$. The fundamental voltage equations in the d and q axes (refer (5) and (6)) are subjected to a modest perturbation to create a small-signal model of PMSM.

$$V_d + \tilde{V_d} = R_s(i_d + \tilde{i_d}) + L_d\frac{d}{dt}(i_d + \tilde{i_d}) - \omega_s L_q(i_q + \tilde{i_q}) \tag{43}$$

$$V_q + \tilde{V_q} = R_s(i_q + \tilde{i_q}) + L_q\frac{d}{dt}(i_q + \tilde{i_q}) + \omega_s[L_d(i_d + \tilde{i_d}) + \psi_{af}] \tag{44}$$

$\tilde{V_d}$, $\tilde{V_q}$, $\tilde{i_d}$, and $\tilde{i_q}$ are the d-q axis stator voltage ripple and stator current ripple respectively. Stator voltage ripple is derived as in (45) and (46) by extracting the ripple terms from (43) and (44).

$$\tilde{V_d} = R_s(\tilde{i_d}) + L_d\frac{d}{dt}\tilde{i_d} - \omega_s L_q\tilde{i_q} \tag{45}$$

$$\tilde{V_q} = R_s(\tilde{i_q}) + L_q\frac{d}{dt}\tilde{i_q} + \omega_s L_d\tilde{i_d} \tag{46}$$

In comparison to the second term, which has a differential element, the effect of the first and last term is minimal and therefore neglected.

$$\tilde{i_d} = \frac{1}{L_d}\int_0^t \tilde{V_d}dt \quad \text{and} \quad \tilde{i_q} = \frac{1}{L_q}\int_0^t \tilde{V_q}dt \tag{47}$$

As the integral of stator voltage ripple is stator flux ripple, the stator current ripple along the d-q axis is defined as in (48).

$$\tilde{i_d} = \frac{\tilde{\psi_d}}{L_d} \quad \text{and} \quad \tilde{i_q} = \frac{\tilde{\psi_q}}{L_q} \tag{48}$$

Then the torque equation can be written as,

$$\tilde{T_e} = \frac{3}{2}\frac{P}{2}\psi_{af}\frac{\tilde{\psi_q}}{L_q}. \tag{49}$$

where $\tilde{\psi_q}^2$ is given in (26).

The torque band can be analytically calculated for different operating conditions by,

$$\frac{d\tilde{T_e}}{dV_{ref}} = 0 \tag{50}$$

$$\tilde{\psi}_q = \begin{cases} -V_{ref}t, \text{ for } 0 \le \hat{A}t \le 0.5T_z \\ -0.5V_{ref}T_z + [cos\alpha - V_{ref}]t_a, \text{ for } 0.5T_z \le \hat{A}t \le (0.5T_z + T_1) \\ -0.5V_{ref}T_z + [cos\alpha - V_{ref}]T_1 + [cos(60-\alpha) - V_{ref}]t_b, \text{ for } (0.5T_z + T_1) \le t \le (T_s - 0.5T_z) \\ 0.5V_{ref}T_z + -V_{ref}t_c, \text{ for } (T_s - 0.5T_z) \le t \le T_s \end{cases} \tag{24}$$

$$\tilde{\psi}_d = \begin{cases} 0, \text{ for } 0 \le t \le 0.5T_z \\ sin(\alpha)t_a, \text{ for } 0.5T_z \le t \le (0.5T_z + T_1) \\ sin(\alpha)T_1 - sin(60-\alpha)t_b, \text{ for } (0.5T_z + T_1) \le t \le (T_s - 0.5T_z) \\ 0, \text{ for } (T_s - 0.5T_z) \le t \le T_s \end{cases} \tag{25}$$

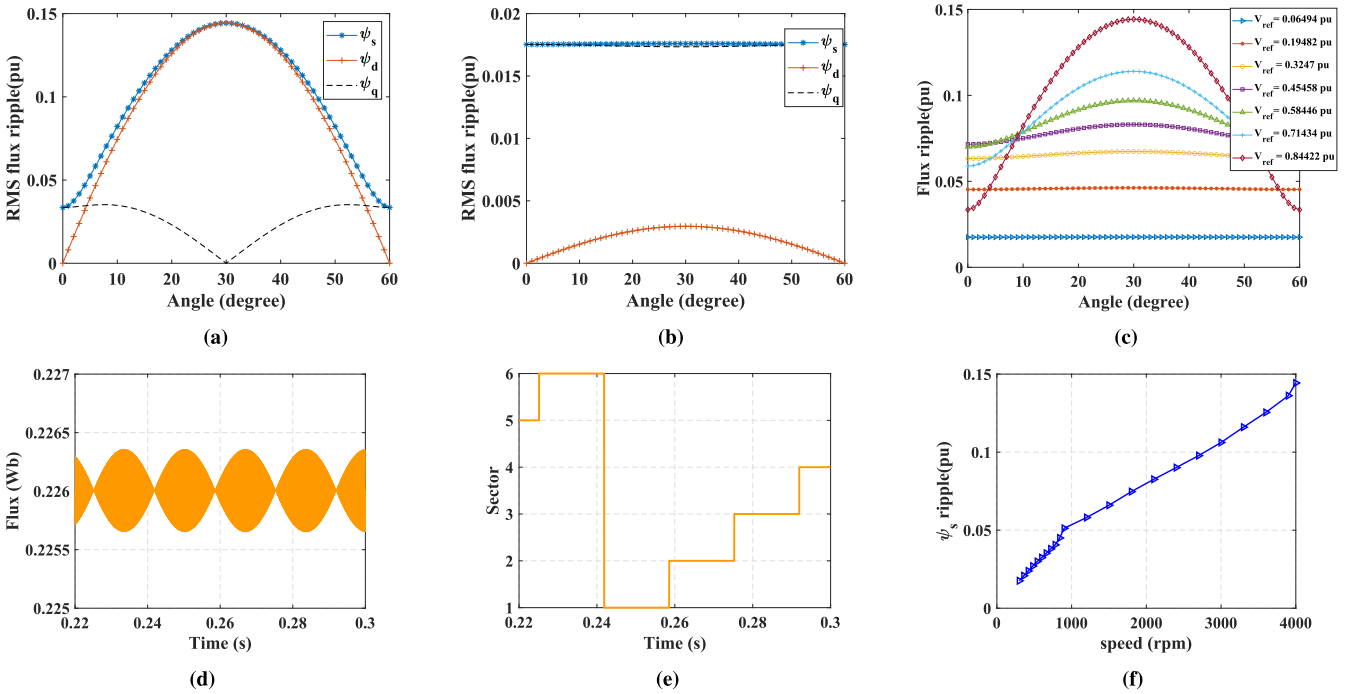

FIGURE 8. Variation of rms flux ripple ($\tilde{\psi}_s, \tilde{\psi}_d, \tilde{\psi}_q$) in a sector for different V_{ref} (a)$V_{ref} = 0.866$ pu(b)$V_{ref} = 0.065$ pu (c)Variation of rms flux ripple in a sector for different speed conditions: Experimentally obtained (d)flux (e) sector for FOC at a speed of 300 rpm (f) Maximum value of $\tilde{\psi}_s$ (p.u.) for different speed conditions in a sector (for ψ_s at $\alpha = 30°$).

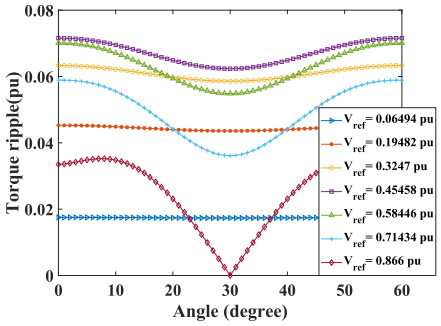

FIGURE 9. Variation of rms torque ripple in a sector for different speed conditions.

As in the previous case, here also, since Q_1, Q_2, and Q_z terms are involved in $\tilde{\psi}_q$ and contain trigonometric functions, this equation turned out to be a transcendental equation which increases the computational burden. So, a simple method is adopted for finding the torque band.

Fig.9 shows the variation of $\tilde{T}_e$ for different V_{ref} in a sector and the analysis concludes that the maximum value occurs at $\alpha = 0°$ and $\alpha = 60°$ (except for the very high speed above 3650 rpm which is close to the rated speed and so the assumption is valid). The torque pattern for FOC shows the exact pattern as predicted by the analytical equation and is given in Fig.10a along with its sector information in Fig.10b. By putting $\alpha = 0°$, the final equation for $\tilde{\psi}_q{}^2$ is given as (51),

Using $\tilde{\psi}_q$, the maximum value of $\tilde{T}_e$ for different speed conditions is calculated analytically and is plotted Fig.10c and is used as the pattern of torque band variations in the proposed method.

$$\begin{aligned}\tilde{\psi}_q{}^2 = &\frac{1}{3}(0.5Q_Z)^2\frac{T_Z}{2T_s} + \frac{1}{3}[(0.5Q_Z)^2 + 0.5Q_Z(0.5Q_Z + 1 - V_{ref}) \\ &+ (0.5Q_Z + 1 - V_{ref})^2]\frac{T_1}{T_s} + \frac{1}{3}[(0.5Q_Z + 1 - V_{ref})^2 \\ &- (0.5Q_Z + 1 - V_{ref})0.5Q_Z + (-0.5Q_Z)^2]\frac{T_2}{T_s} \\ &+ \frac{1}{3}(-0.5Q_Z)^2\frac{T_Z}{2T_s}. \end{aligned} \tag{51}$$

$\tilde{\psi}_q$ in (51) depends only on V_{ref}. So, this proposed equation is a generalized form applicable to any type of motor.

D. PROPOSED DTC SCHEMES WITH SLIDING BANDS

In Fig.11, a block diagram of the full control system is presented. Hysteresis controllers with sliding bands are utilized in the proposed scheme. In this paper, two novel patterns of torque and flux hysteresis bands are adopted named Scheme 1 and Scheme 2, and use the same block schematic as given in Fig.11

The flux reference is calculated from the torque reference using MTPA (Maximum Torque Per Ampere) control and the flux error is applied to the flux hysteresis comparator with sliding band. The maximum value of $\tilde{\psi}_s$ (p.u.) and $\tilde{T}_e$ (p.u.) are converted into the corresponding bands for different speed

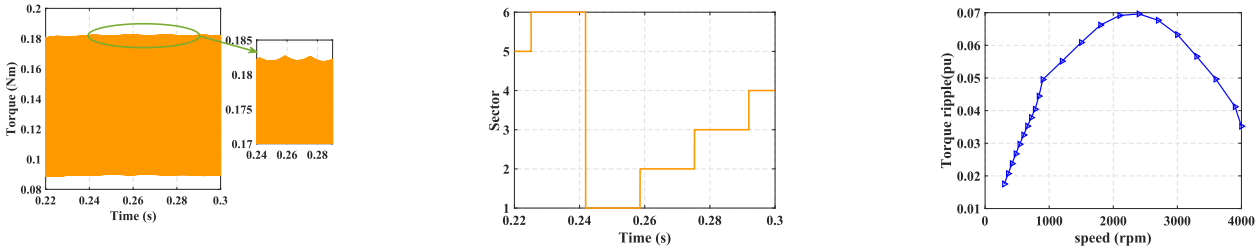

FIGURE 10. Experimentally obtained (a) torque (b) sector for FOC at a speed of 300 rpm (c) Maximum value of $\tilde{T_e}(p.u.)$ for different speed conditions in a sector (for ψ_s at $\alpha = 30°$).

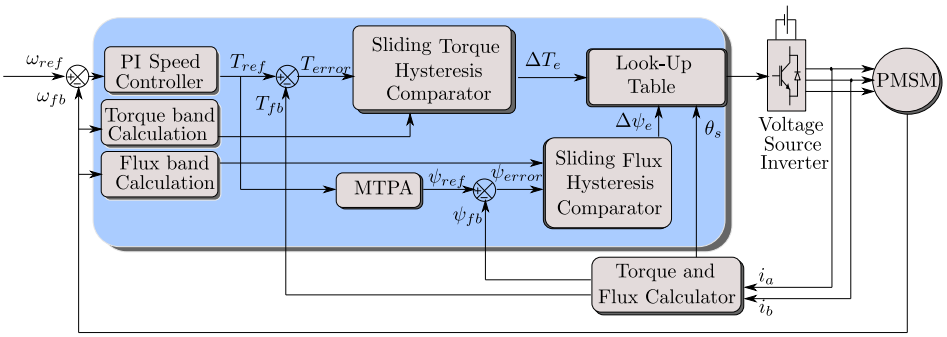

FIGURE 11. Block diagram of proposed DTC scheme.

conditions and the same is shown in Fig.12a. Motor speed information is also needed for accurate variation of torque and flux band as shown in the block diagram (Fig.11). From the Fig.12a, it is found that if the analytically obtained torque band and flux bands are used in the entire speed range of operations, there are operating points where the bands go above the band set for conventional DTC (torque band=12% of the rated torque and flux band = 0.001 Nm). So, in this paper, two different variations of torque bands and flux bands are selected.

- **Scheme 1:** In scheme 1, the exact analytically obtained band for flux and torque is set and the variation of the same is given in Fig.12a.
- **Scheme 2:** The maximum torque band is limited at 12% of the rated torque and the maximum flux band is fixed at 0.001Wb and the variation of both the bands with speed is given in Fig.12b.

The efficacy of the two proposed schemes is experimentally validated and the results are discussed in section IV.

IV. EXPERIMENTAL RESULTS AND DISCUSSION

A photograph of the laboratory setup of the experiment is shown in Fig.13. The experiment is carried out on a 1.07 kW, 300 V, 50 Hz, three-phase PMSM fed from an insulated-gate bipolar transistor (IGBT) based voltage source inverter (VSI). The parameters of the experimented motor used in this paper are detailed in Table.2.

WAVECT with an FPGA controller and in-built current and voltage sensors are used for implementing the control algorithms and generating the PWM signals. The experimental results of the proposed methods are discussed in the coming sections.

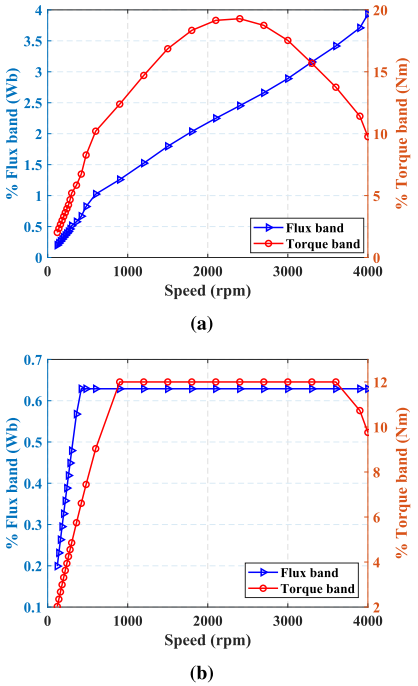

FIGURE 12. Analytically obtained variation of torque and flux band with reference to FOC for different speed regions (a) Scheme 1 DTC (b) Scheme 2 DTC.

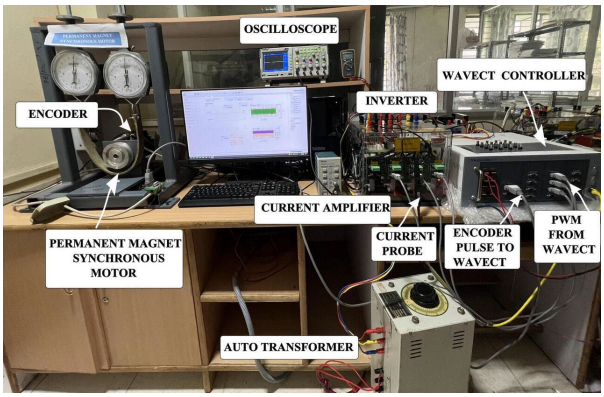

FIGURE 13. Laborartory set-up for the DTC controlled surface mounted PMSM.

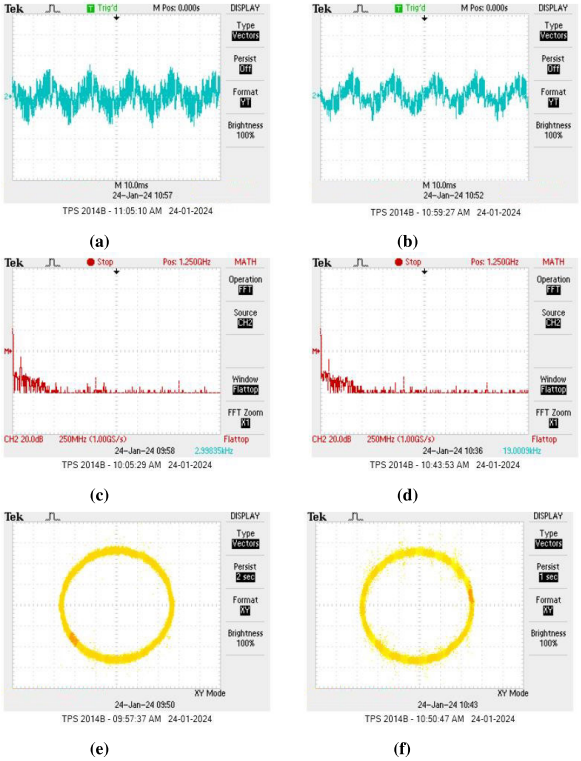

FIGURE 14. Experimentally obtained current, frequency spectrum and stator flux trajectory for a speed of 300 rpm (a),(c), and (e) Conventional DTC (b),(d), and (f) Scheme 1 DTC.

TABLE 2. Parameters of PMSM used.

Motor Parameters	Values
Rated Power (P_m)	1.07 kW
Base Speed (N)	4000 rpm
Stator Resistance per phase (R_s)	1.1 Ω
Stator inductance along d-axis (L_d)	8.2 mH
Stator inductance along q-axis (L_q)	8.2 mH
Inertia (J)	0.000554 Kg.m^2
No.of Poles (P)	4

A. EXPERIMENTAL RESULTS PERTAINING TO CONVENTIONAL DTC AND PROPOSED SCHEMES

The torque and flux band are varied in accordance with the FOC scheme as given by (42) and (49). Fig.14 and

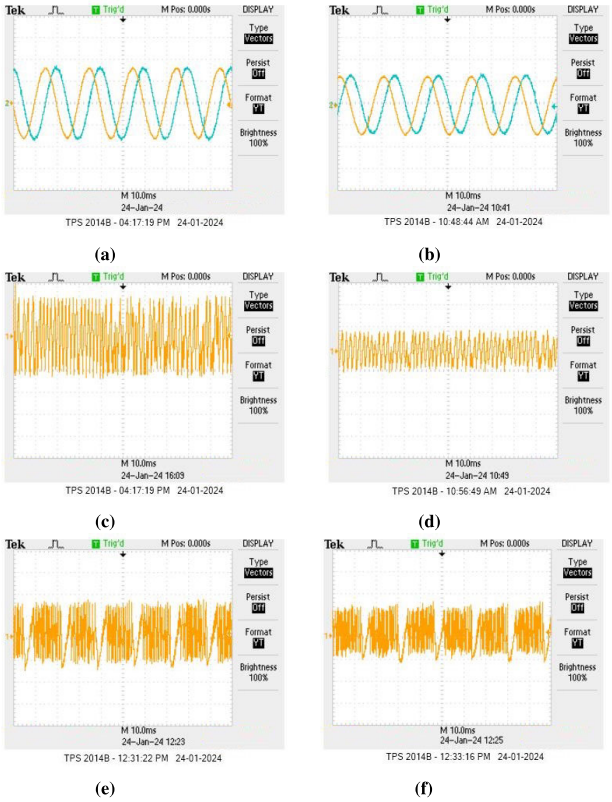

FIGURE 15. Experimentally obtained flux in $\alpha - \beta$ frame, torque error and flux error for a speed of 300 rpm (a),(c), and (e) Conventional DTC (b),(d), and (f) Scheme 1 DTC.

Fig.15 show the experimentally obtained waveforms for a fundamental frequency of 10 Hz (300 rpm) pertaining to conventional DTC and the proposed DTC schemes. With the conventional DTC scheme, the motor is not running below a speed of 300 rpm, so, for better comparison, the waveforms in Fig.14 and Fig.15 are taken at 300 rpm. The current waveform in Fig.14a for the conventional DTC scheme is having high THD of 80.54% and its corresponding frequency spectrum is given in Fig.14c. This is very high THD as far as the low-speed operation is concerned. Fig.14b shows the current waveform for the scheme 1 DTC for a fundamental frequency of 10 Hz (300 rpm). The distortion in current is reduced and the frequency spectrum pertaining to this operating point is shown in Fig.14d. The frequency spectrum shows a remarkable reduction in the current THD.

Scheme 1 achieves a current THD of 43.25%, which is a 46.29 % reduction from the conventional DTC scheme. The stator flux trajectory of the conventional DTC and Scheme 1 DTC is depicted in Fig.14e and Fig.14f respectively. It is evident that the trajectory is getting smooth in the proposed DTC scheme compared to the conventional scheme. To show further efficacy of the proposed scheme, the stator flux estimated in $\alpha - \beta$ frame of conventional DTC and the proposed scheme 1 is given in Fig.15a and Fig.15b. The sliding of the bands is carried out in such a way that the low-speed regions are provided with low bands. To show

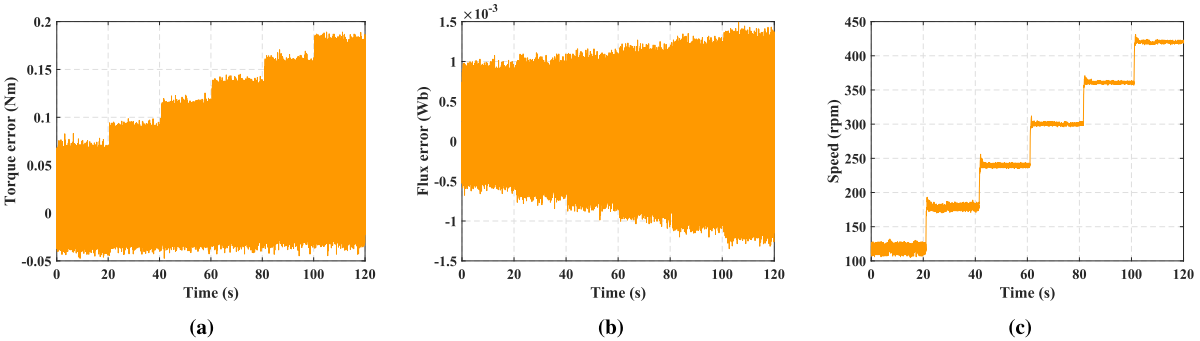

FIGURE 16. Experimentally (a) Torque band variation (b) flux band variation (c) speed variation.

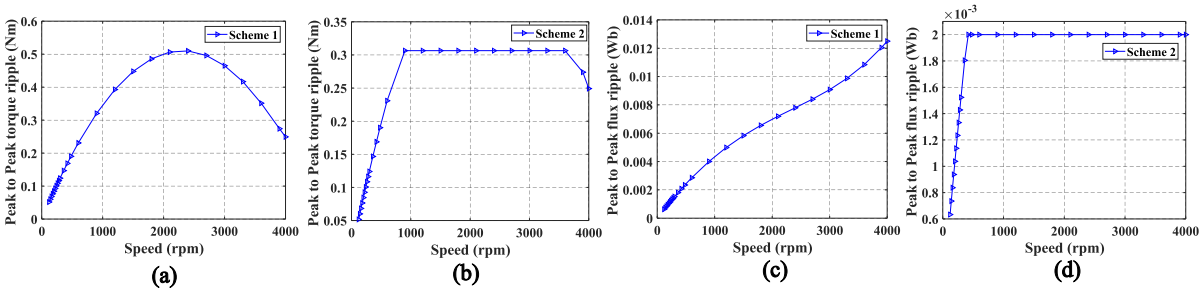

FIGURE 17. Experimentally obtained Peak-to-peak torque ripple (a) Scheme 1 (b) Scheme 2 and Peak-to-peak flux ripple (c) Scheme 1 (d) Scheme 2.

the reduction in the torque band, the torque error of the conventional DTC scheme and the proposed scheme 1 DTC are depicted in Fig.15c and Fig.15d respectively. It is clear from Fig.15d that the torque error is getting reduced. Similarly, the flux error for the conventional DTC and the proposed scheme is depicted in Fig.15c and Fig.15d respectively, which clearly show the reduction in the flux error.

The experimental validation of sliding of the torque band and flux band for different speed conditions are depicted in Fig.17, Fig.16b, and Fig.16c. Initially the speed is given as 120 rpm and is increased to 180 rpm after 20 seconds. A corresponding shift in the torque band and flux band is seen in Fig.16a and Fig.16b respectively, and the corresponding speed change is given in Fig.16c. After each 20 seconds, a step change in speed is given and the increment in the bands is well evident from the plot. Scheme 1 and Scheme 2 differ only in regions where the band goes beyond the conventional scheme. In the low-speed regions, both schemes have equal hysteresis bands, and hence the current waveforms, frequency spectrum, and flux trajectories are the same. Peak-to-peak torque ripple and peak-to-peak flux ripple of the proposed scheme 1 and scheme 2 are shown in Fig.17. Under the low-speed regions, the torque ripple as well as the flux ripple is reduced in both the proposed schemes. With the narrowing of the flux and torque bands, the average switching frequency may increase. However, it is known that the average switching frequency of the conventional DTC scheme is less in the low-speed region. It is verified that the narrowing of bands restricts the average switching frequency within the working limits and is hence compatible with the current thermal design.

B. COMPARISON WITH DIFFERENT CONTROL SCHEMES

In this section, a comparison of the proposed schemes is carried out with conventional DTC and FOC under no-load conditions. In Fig.18a, the current THD for proposed scheme 1 and scheme 2 is compared with conventional schemes for the entire speed range. Fig.18b shows the zoomed version of Fig.18a in the low-speed range. It is seen that the conventional DTC is unable to run the motor at the low-speed region up to a speed of 300 rpm, marked as 'Non operating region'. At 300 rpm, the THD for the conventional DTC scheme is 80.54 % and is reduced to 43.25% with Scheme 1, which brings a 46.299 % THD reduction. Since the band pattern of scheme 2 is similar to scheme 1 in the very low-speed range, the THD characteristics also show a similar variation. The zoomed version of Fig 18a in the medium and high-speed region is presented in Fig 18c. From a medium speed range, the band pattern of the two proposed schemes is different and it is seen that scheme 2 performs better compared to scheme 1 and the conventional DTC scheme. In the high-speed regions, scheme 2 adopts the band pattern similar to the conventional DTC scheme and is found to be better compared to the other schemes under consideration. The switching frequencies of all the schemes are compared and presented in Fig.18d. Due to the presence of hysteresis controllers, the switching frequency of the DTC schemes

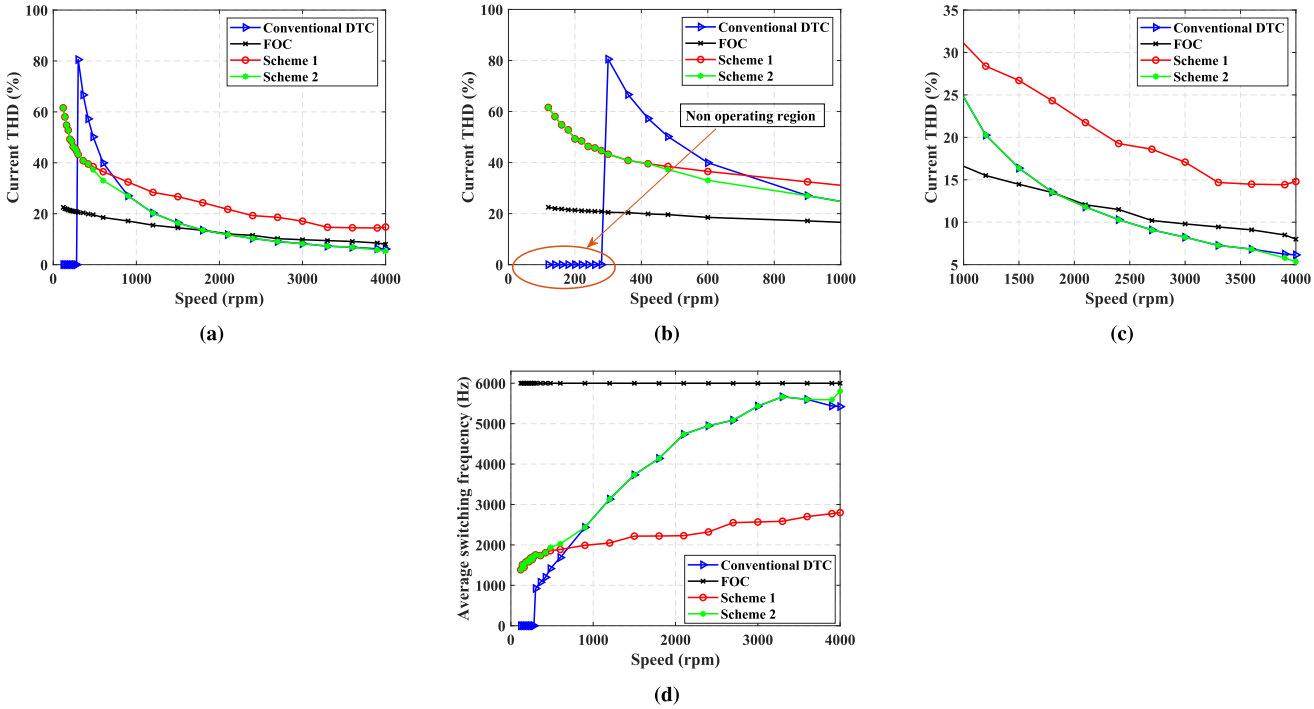

FIGURE 18. Experimental comparison of current THD of Scheme 1 and Scheme 2 with conventional DTC and FOC (a) For the entire speed range(b) under low- speed(c)under medium and high speed (d)switching frequency comparison.

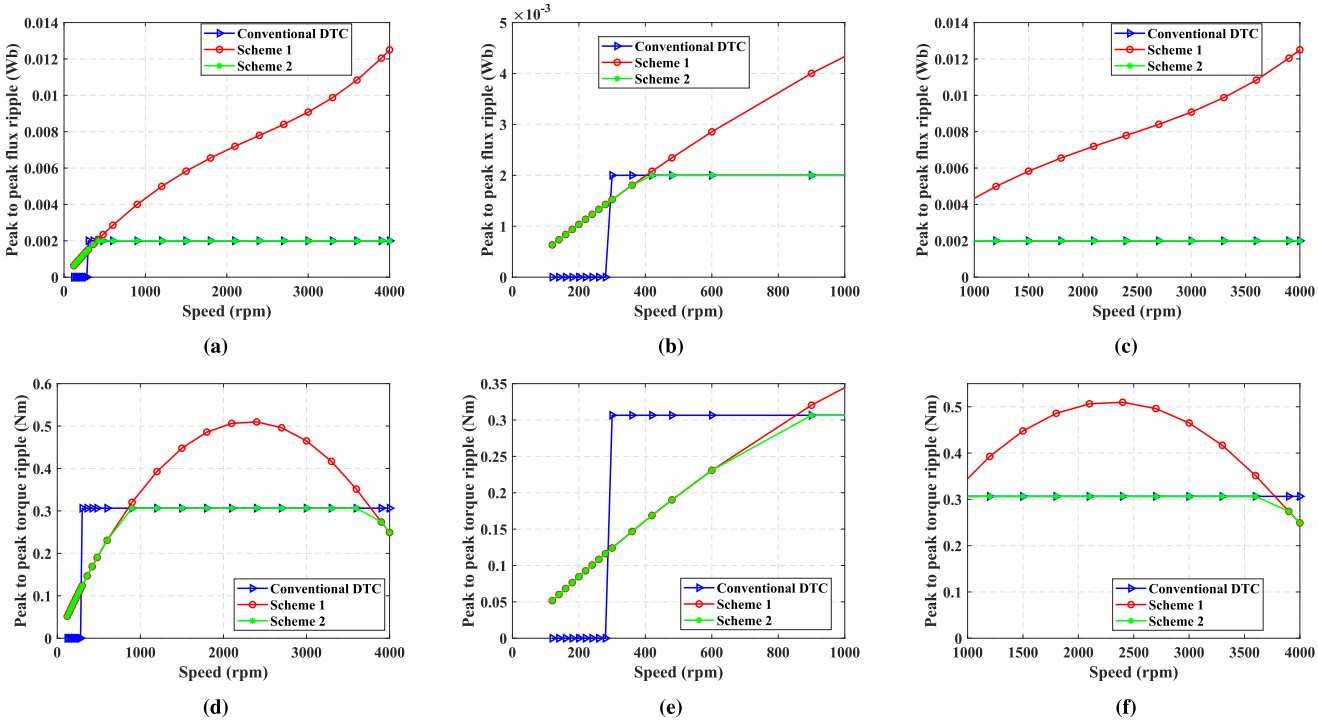

FIGURE 19. Experimental comparison of Scheme 1 and Scheme 2 with conventional DTC (a) Peak to peak flux ripple of for the entire speed range (b) Peak to peak flux ripple under low-speed(c)Peak to peak flux ripple under medium and high speed (d) Peak to peak torque ripple of for the entire speed range(e) Peak to peak torque ripple under low-speed(f)Peak to peak torque ripple under medium and high speed.

is variable and hence average switching frequency is taken for comparison. The torque and flux bands were calculated from the FOC scheme with a constant switching frequency of 6 kHz. Under low speed, only a marginal increment in the

TABLE 3. Comparative analysis of the proposed scheme with other schemes in the literature.

Reference Paper	Is applicable to all motors	Controlling bands	Computational burden	Logic behind Torque band calculation	Logic behind Flux band calculation	MTPA used	Switching frequency	Difficulty level in calculating bands
[21]	No	both flux band and torque band	High	Systematic	Trial and error	No	constant	High
[25]	Yes	only torque band	Low	Random	fixed as conventional	No	Variable and high	Low
[26]	Yes	only torque band	Low	Random	fixed as conventional	No	Variable	Low
[27]	No	sample time	Low	fixed as conventional	fixed as conventional	No	Variable	Low
Proposed method	Yes	both flux band and torque band	Low	Systematic	Systematic	Yes	Variable	low

switching frequency is seen with DTC scheme 1 and scheme 2 compared to conventional DTC.

For better comparison, the peak-to-peak flux ripple and the peak-to-peak torque ripple of the proposed schemes are compared with the conventional DTC and are presented in Fig.19. The low-speed region of Fig.19a is zoomed in Fig.19b, where the peak-to-peak flux ripple is very much reduced for the proposed two schemes. Fig.19c corresponds to the medium and high-speed regions where scheme 2 is having a reduced peak-to-peak flux ripple. Though scheme 1 DTC performs better in terms of peak-to-peak torque ripple under low speeds, its performance is not satisfactory under medium and high speeds whereas scheme 2 performs better compared to scheme 1 in the entire operating region. Fig.19d shows the peak-to-peak torque ripple of the proposed schemes along with the conventional DTC scheme. The low-speed region is zoomed and is presented in Fig.19e, whereas the medium and high-speed region is presented in Fig.19f. Both the proposed schemes have low peak-to-peak torque ripple in the low-speed region of operation. But under high speed, scheme 1 exhibits more ripple compared to scheme 2.

To critically evaluate the effectiveness of the proposed method, a comprehensive comparison of four related works published in the literature is summarized in Table 3. In a DTC-controlled PMSM motor drive, the technique put forth by Mathapati et al. [21] provides an analytical and offline way of determining the hysteresis bands for the torque and flux hysteresis comparator. To enhance the flux regulation in a DTC-hysteresis-based induction machine at low speeds, two dynamic hysteresis bands are suggested by Alsofyani et al. [25]. To address the flux droop in a low-rotor-speed range, a modified flux regulation approach for the classical DTC utilizing a single torque hysteresis band is proposed as a modification to the paper [26], whereas in [27], the variable nature of torque hysteresis band is obtained by reducing the sample time. So, from Table 3, it can be seen that the proposed method outperforms other related works in terms of various performance parameters.

V. CONCLUSION

This article details the difficulties associated with PMSMs while operating with conventional DTC schemes, especially under low-speed regions. Since the torque and flux hysteresis bands of a conventional DTC are fixed in the entire speed range, its performance becomes worse in the low-speed region due to increased torque and flux ripples. Consequently, current THD is seen to be very high under low speed and hence exhibits starting issues. In this paper, two DTC schemes are proposed with a novel sliding pattern for both torque and flux hysteresis bands. Sliding of both torque and flux hysteresis controllers is carried out most generically so that it can be applied to any motor. The proposed approach not only reduces the current THD but reduces torque ripple and flux ripple also. The proposed approach reduces the current THD without affecting the switching frequency increment and reduces torque ripple and flux ripple. The proposed method is analytically evaluated and experimentally validated on a 1.07 kW SPMSM using a WAVECT FPGA controller. The results of the experiment confirm that the proposed schemes are effective in reducing the current THD, torque ripple, and flux ripple which enables smooth motor operation at low-speed regions with only a marginal increment in the switching frequency.

A. CONFLICT OF INTEREST

The corresponding author declares that no pertinent financial or non-financial interests are to be disclosed on behalf of all authors.

REFERENCES

[1] I. Takahashi and T. Noguchi, "A new quick-response and high-efficiency control strategy of an induction motor," *IEEE Trans. Ind. Appl.*, vol. IA-22, no. 5, pp. 820–827, Sep. 1986.
[2] C. Lascu, I. Boldea, and F. Blaabjerg, "A modified direct torque control for induction motor sensorless drive," *IEEE Trans. Ind. Appl.*, vol. 36, no. 1, pp. 122–130, Jun. 2000.
[3] Y.-S. Lai and J.-H. Chen, "A new approach to direct torque control of induction motor drives for constant inverter switching frequency and torque ripple reduction," *IEEE Trans. Energy Convers.*, vol. 16, no. 3, pp. 220–227, Jul. 2001.
[4] L. Tang, L. Zhong, M. F. Rahman, and Y. Hu, "A novel direct torque controlled interior permanent magnet synchronous machine drive with low ripple in flux and torque and fixed switching frequency," *IEEE Trans. Power Electron.*, vol. 19, no. 2, pp. 346–354, Mar. 2004.
[5] A. K. Peter, J. Mathew, and K. Gopakumar, "A simplified DTC-SVPWM scheme for induction motor drives using a single PI controller," *IEEE Trans. Power Electron.*, vol. 38, no. 1, pp. 750–761, Jan. 2023.
[6] A. Mohan, M. Khalid, and A. C. Binojkumar, "Performance analysis of permanent magnet synchronous motor under DTC and space vector-based DTC schemes with MTPA control," in *Proc. Int. Conf. Commun., Control Inf. Sci. (ICCISc)*, vol. 1, Jun. 2021, pp. 1–8.
[7] G. J. Capella, J. Pou, S. Ceballos, G. Konstantinou, J. Zaragoza, and V. G. Agelidis, "Enhanced phase-shifted PWM carrier disposition for interleaved voltage-source inverters," *IEEE Trans. Power Electron.*, vol. 30, no. 3, pp. 1121–1125, Mar. 2015.

[8] D. Mohan, X. Zhang, and G. H. Beng Foo, "Generalized DTC strategy for multilevel inverter fed IPMSMs with constant inverter switching frequency and reduced torque ripples," *IEEE Trans. Energy Convers.*, vol. 32, no. 3, pp. 1031–1041, Sep. 2017.
[9] S. A. A. Tarusan, A. Jidin, M. L. M. Jamil, K. A. Karim, and T. Sutikno, "A review of direct torque control development in various multilevel inverter applications," *Int. J. Power Electron. Drive Syst. (IJPEDS)*, vol. 11, no. 3, p. 1675, Sep. 2020.
[10] S. K. Chien, "Enhanced DTC induction motor drives for THD minimization performance improvement with multilevel inverter," *Int. J. Power Electron. Drive Syst. (IJPEDS)*, vol. 13, no. 1, p. 93, Mar. 2022. [Online]. Available: https://api.semanticscholar.org/CorpusID:247309343
[11] S. Lakhimsetty, V. S. P. Satelli, R. S. Rathore, and V. T. Somasekhar, "Multilevel torque hysteresis-band based direct-torque control strategy for a three-level open-end winding induction motor drive for electric vehicle applications," *IEEE J. Emerg. Sel. Topics Power Electron.*, vol. 7, no. 3, pp. 1969–1981, Sep. 2019.
[12] Y. Zahraoui, M. Akherraz, and C. Fahassa, "Induction motor DTC performance improvement by reducing torque ripples in low speed," *UPB Sci. Bull., Ser. C*, vol. 81, no. 3, pp. 249–260, 2019.
[13] D. Casadei, G. Serra, and A. Tani, "The use of matrix converters in direct torque control of induction machines," *IEEE Trans. Ind. Electron.*, vol. 48, no. 6, pp. 1057–1064, Aug. 2001.
[14] M. Deshpande, M. S. Kumaran, and R. Muthu, "Direct torque control of the direct three level matrix converter based on induction motor drive," *Rev. Téc. Ing. Univ. Zulia.*, vol. 39, no. 11, pp. 194–204, 2016.
[15] S. S. Sebtahmadi, H. Pirasteh, S. H. A. Kaboli, A. Radan, and S. Mekhilef, "A 12-sector space vector switching scheme for performance improvement of matrix-converter-based DTC of IM drive," *IEEE Trans. Power Electron.*, vol. 30, no. 7, pp. 3804–3817, Jul. 2015.
[16] N. M. Nordin, N. R. N. Idris, and N. A. Azli, "Direct torque control with 5-level cascaded H-bridge multilevel inverter for induction machines," in *Proc. IECON 37th Annu. Conf. IEEE Ind. Electron. Soc.*, Nov. 2011, pp. 4691–4697.
[17] A. Joshua Dasamma and S. Arumugam, "A novel lookup table based model predictive torque control strategy using matrix converter suitable for permanent magnet synchronous motor fed marine electric propulsion drives," *Optim. Control Appl. Methods*, vol. 43, no. 5, pp. 1520–1545, Sep. 2022.
[18] A. Mohan, M. Khalid, and A. Binojkumar, "An investigation into the applications of real-time simulator in experimental validation of PMSM-based electric drive system," in *Proc. Int. Conf. Adv. Electr. Comput. Technol.* Singapore: Springer, 2021, pp. 1091–1107.
[19] C. Xia, J. Zhao, Y. Yan, and T. Shi, "A novel direct torque control of matrix converter-fed PMSM drives using duty cycle control for torque ripple reduction," *IEEE Trans. Ind. Electron.*, vol. 61, no. 6, pp. 2700–2713, Jun. 2014.
[20] D. Casadei, G. Grandi, G. Serra, and A. Tani, "Effects of flux and torque hysteresis band amplitude in direct torque control of induction machines," in *Proc. IECON94 20th Annu. Conf. IEEE Ind. Electron.*, vol. 1, 1994, pp. 299–304.
[21] S. Mathapati and J. Bocker, "Analytical and offline approach to select optimal hysteresis bands of DTC for PMSM," *IEEE Trans. Ind. Electron.*, vol. 60, no. 3, pp. 885–895, Mar. 2013.
[22] G. Narayanan and V. T. Ranganathan, "Analytical evaluation of harmonic distortion in PWM AC drives using the notion of stator flux ripple," *IEEE Trans. Power Electron.*, vol. 20, no. 2, pp. 466–474, Mar. 2005.
[23] M. Khalid, A. Mohan, and A. C. Binojkumar, "Carrier-based variable frequency PWM technique for PMSM drives to achieve dispersed spectrum and extended low-speed operation capability," *Arabian J. Sci. Eng.*, vol. 48, no. 11, pp. 15045–15061, Nov. 2023.
[24] M. Khalid, A. Mohan, P. P. Pullukkara, and A. C. Binojkumar, "A modified variable switching frequency spread-spectrum PWM technique with reduced torque ripple for a vector-controlled PMSM drive," *IEEE Access*, vol. 10, pp. 132800–132813, 2022.
[25] I. M. Alsofyani, N. R. N. Idris, and K.-B. Lee, "Dynamic hysteresis torque band for improving the performance of lookup-table-based DTC of induction machines," *IEEE Trans. Power Electron.*, vol. 33, no. 9, pp. 7959–7970, Sep. 2018.
[26] I. M. Alsofyani, K. Y. Kim, S. S. Lee, and K.-B. Lee, "A modified flux regulation method to minimize switching frequency and improve DTC-hysteresis-based induction machines in low-speed regions," *IEEE J. Emerg. Sel. Topics Power Electron.*, vol. 7, no. 4, pp. 2346–2355, Dec. 2019.
[27] K. B. Mohanty, "A direct torque controlled induction motor with variable hysteresis band," in *Proc. 11th Int. Conf. Comput. Model. Simul.*, 2009, pp. 405–410.

ANJALY MOHAN (Student Member, IEEE) received the B.Tech. degree in electrical and electronics engineering from the Saintgits College of Engineering, Mahatma Gandhi University, Kottayam, India, in 2012, and the M.Tech. degree in power electronics and control from the Government Engineering College Idukki, in 2015. She is currently pursuing the Ph.D. degree with the Rajiv Gandhi Institute of Technology, Kottayam, under APJ Abdul Kalam Technological University, Thiruvananthapuram, India. Her research interests include direct torque control technique and permanent magnet synchronous motor drives.

MEERA KHALID received the B.Tech. degree in electrical and electronics engineering from the Mar Athanacius College of Engineering, Kothamangalam, in 2003, and the M.Tech. degree in industrial drives and control from the Government Rajiv Gandhi Institute of Technology, Kottayam, under APJ Abdul Kalam Technological University, Thiruvananthapuram, Kerala, India, in 2011, where she is currently pursuing the Ph.D. degree in motor drives and control with the Department of Electrical Engineering. Her research interests include pulse width modulation techniques and electrical drives.

A. C. BINOJKUMAR (Senior Member, IEEE) received the B.Tech. degree in electrical and electronics engineering from the Rajiv Gandhi Institute of Technology, Kottayam, India, in 1998, the M.Tech. degree from the College of Engineering, Thiruvananthapuram, India, in 2001, and the Ph.D. degree from the Indian Institute of Science, Bengaluru, India, in 2016. He is currently a Professor with the Government Engineering College Idukki, Kerala, India. His research interests include pulse width modulation techniques, electrical drives, and motor acoustic noise. He is a reviewer of various international journals and conferences.